THE APPLICATION OF LASER-ABLATION MICROPROBE – INDUCTIVELY COUPLED PLASMA – MASS SPECTROMETRY (LAM–ICP–MS) TO IN SITU TRACE-ELEMENT DETERMINATIONS IN MINERALS

SIMON E. JACKSON, HENRY P. LONGERICH, GREG R. DUNNING AND BRIAN J. FRYER

*Department of Earth Sciences and Centre for Earth Resources Research, Memorial University of Newfoundland,
St. John's, Newfoundland A1B 3X5*

ABSTRACT

A laser ablation microprobe (LAM) sample-introduction system, designed for *in situ* microsampling of minerals in petrographic sections, has been interfaced to an Inductively Coupled Plasma – Mass Spectrometer (ICP–MS). The LAM consists of a Q-switched Nd:YAG laser with power attenuation and steering optics to guide the laser beam through the phototube of a petrographic microscope, where it is focused onto the petrographic section contained in a sample cell. The response of rock-forming minerals to ablation is related to their absorptivity of the 1064 nm wavelength of the laser beam (a function of the proportion of transition elements, especially Fe), and their physical properties, particularly cleavage and tenacity. Minerals with a high absorptivity can generally be ablated controllably in thin section. In minerals with low absorptivity, catastrophic ablation may occur due to absorption at interfaces beneath the mineral surface, particularly at the mineral – glass slide interface in standard thin sections. Most minerals can be ablated controllably in unsupported polished wafers, grain mounts and polished blocks, where ablation pits with diameters of 20–40 μm can be achieved routinely. In addition, the ability of the LAM to bore allows production of vertical profiles of element concentrations at a much finer spatial resolution. Comparison of LAM- and solution-ICP–MS analyses of titanite, zircon, apatite, uraninite, and garnet separates demonstrates that a simple scheme of calibration employing a spiked NBS silicate glass reference material, using major-element internal standards to correct for differences in ablation yield, drift, and matrix effects, provides good accuracy and precision (RSD < 10%, at concentrations > 60 ppm) for a diverse suite of elements. Routine limits of detection are about 0.5 ppm.

Keywords: laser ablation, microprobe, ICP–MS, *in situ* trace-element analysis, *REE*, horizontal and vertical zoning.

SOMMAIRE

Une microsonde au laser conçue pour ablation, munie d'un système d'introduction d'échantillons pour micro-échantillonage de minéraux à partir d'une lame mince, a été intégrée à un système de plasma à couplage inductif avec spectromètre de masse. On peut atténuer la puissance du laser Nd:YAG à polarité Q et en assurer la collimation optique pour le guider à travers le tube photographique d'un microscope polarisant, pour qu'il soit focalisé sur une lame mince dans une chambre logeant l'échantillon. La réponse des minéraux courants à l'ablation est fonction de leur absorptivité du faisceau d'une longueur d'onde de 1064 nm, qui à son tour est fonction de la teneur en éléments de transition, surtout le Fe, et des propriétés physiques des minéraux, particulièment la présence de clivages et la ténacité. L'ablation des minéraux à absorptivité élevée peut être controllée, en général. Dans le cas de ceux dont l'absorptivité est faible, l'ablation peut s'avérer catastrophique à cause d'une absorption au dessous de la surface, surtout à l'interface entre minéral et la plaque de verre du porte-échantillon. Pour la plupart des minéraux, l'ablation peut être controllée en utilisant une section polie sans support ou des agrégats de grains en blocs polis; nous pouvons produire couramment un cratère d'ablation d'un diamètre entre 20 et 40 μm dans ces cas. De plus, l'abilité du rayon laser de forer nous permet d'effectuer un profil vertical des éléments à résolution spatiale très fine. Nous avons effectué une comparaison des résultats obtenus par plasma à couplage inductif avec spectromètre de masse en utilisant le nouveau système et la technique traditionnelle de solutions, sur titanite, zircon, apatite, uraninite et grenat. Avec un simple calibrage fondé sur un verre siliceux de référence NBS, et des étalons internes pour les éléments majeurs, pour corriger les différences en efficacité de l'ablation, déplacement, et effets de matrice, nous obtenons une précision et une justesse satisfaisantes (RSD < 10% à des concentrations de plus de 60 ppm) pour une série d'éléments divers. Le seuil de détection courant est d'environ 0.5 ppm.

(Traduit par la Rédaction)

Mots-clés: ablation au laser, microsonde, plasma à couplage inductif, spectrométrie de masse, analyse *in situ*, éléments traces, terres rares, zonation horizontale, zonation verticale.

INTRODUCTION

The elemental composition of rock-forming minerals has long been studied by mineralogists and petrologists because it can provide valuable information concerning the chemical and physical processes and conditions during, and subsequent to, the formation of rocks and ore deposits. Until recently, the required analytical data have been obtained by separating the minerals from the rock for analysis by conventional methods or by analyzing the minerals in petrographic sections using the electron microprobe. The separation of minerals from the rock matrix is generally extremely laborious and, moreover, does not yield information concerning chemical variations within mineral grains. The electron probe is restricted by high detection-limits (Reed 1990, Potts 1987). More recently, significant advances in the area of trace-element microprobe analysis have been made with the development of Secondary Ion Mass Spectrometry (SIMS), Proton Induced X-Ray Emission (PIXE), and Synchrotron X-Ray Fluorescence (SXRF). These techniques, recently reviewed by Reed (1990), have shown great potential for *in situ* mineral analysis and have demonstrated the need for microprobe techniques capable of determinations at trace-element levels.

The recent coupling of a laser ablation sampling device with an inductively coupled plasma – mass spectrometer (ICP–MS) (Gray 1985, Arrowsmith 1987, Moenke-Blankenburg *et al.* 1990) has yielded a relatively simple and inexpensive instrument capable of direct analysis of elemental and isotope ratios in solid samples with extremely low limits of detection. Although laser ablation has been developed largely as a direct bulk sampling device for homogeneous samples (Denoyer *et al.* 1991), it is clear that it has the potential to be developed as a microprobe for applications requiring high-resolution sampling (Longerich *et al.* 1993).

This paper describes our development of the LAM–ICP–MS for *in situ* trace-element analysis of rock-forming minerals in petrographic sections. Progress in controlling the ablation process and in optimizing spatial resolution for both lateral and vertical chemical profiling is described. The effectiveness of a simple calibration procedure is demonstrated by comparing results of LAM–ICP–MS analyses of a wide variety of mineral separates with results obtained by conventional solution-nebulization ICP–MS. Detection limits are discussed in relation to the controlling parameters.

EXPERIMENTAL

Laser ablation apparatus

The LAM instrumentation has been described briefly by Longerich *et al.* (1993) and is shown schematically in Figure 1. It consists of a Q-switched Nd:YAG laser operated at the fundamental wavelength ($\lambda = 1064$ nm)

in either single-shot mode or at rates of repetition of 2, 5 or 10 Hz. The laser beam is steered from the laser through the photo tube of a petrographic microscope by means of three 45° dielectric mirrors. It is then focused through a silica window onto the sample contained in a cell. The microscope allows operator viewing of the sample using either transmitted or reflected light at a range of magnifications (50 to 200×). A simple plano-convex, fused silica lens (25 mm focal length) is used for ablation at pulse energies greater than about 5 mJ because cemented microscope objectives are suceptible to laser damage at these energies. However, microscope objectives have been used at lower energies without incurring any damage. These lenses have the advantages of producing better images, a greater magnification, and ablation pits of superior quality. While performing ablation, the reflected light and binocular prisms in the microscope are retracted, leaving an optical path to the objective lens that is free of glass optics. The ablation process can then be viewed using a TV camera and monitor.

The laser, as delivered, produces a maximum pulse energy of 320 mJ (9 ns pulse duration). Pulse energy may be attenuated by means of the Q-switch delay potentiometer. However, this control is not sensitive and reproducible at the very low pulse energies required for controlled ablation of most minerals. Deoptimizing the Q-switch delay also results in significant broadening of the laser pulse, which affects ablation characteristics. To reduce the use of this adjustment, a teflon aperture 1.7 mm in diameter was inserted in the resonator cavity of the laser to attenuate the maximum pulse energy to approximately 70 mJ. Then, to provide sensitive control of power at very low energies, the first steering mirror is interchanged with a high-energy laser beam sampler. This, when used in conjunction with a rotatable half-wave plate, acts as an optical attenuator capable of continuously variable reflectance between 2 and 10%. Combining this with limited use of the Q-switch delay adjustment can provide the optimal pulse energy for ablation of all types of mineral (see below). A volume-absorbing power meter can be swung into the laser path to measure the pulse energy (down to about 1 mJ/pulse).

ICP–MS instrument and optimization

The sample is analyzed using a Sciex ELAN model 250 ICP–MS. A flow of argon carries the ablated material from the sample cell through approximately 1.5 m of 3 mm i.d. polyurethane tubing to the ICP torch *via* a sheath gas junction (Beauchemin & Craig 1990) inserted between the spray chamber and the torch. The gas flows to the nebulizer and LAM sample chamber are controlled by separate mass-flow controllers. These arrangements allow rapid switchover between solution nebulization and laser ablation when requested, without altering instrument configuration. Initial installation and early modifications to the ELAN have been described
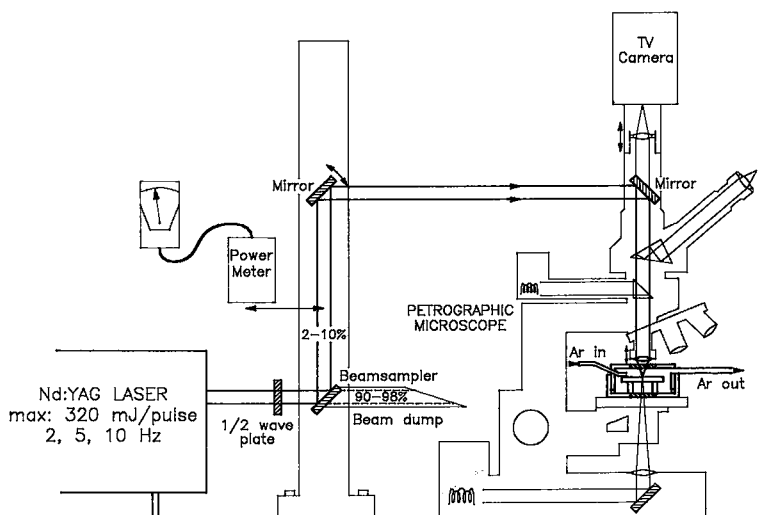
FIG. 1. Schematic of the LAM. In practice, the laser beam enters the microscope from the left-hand side.

by Longerich *et al.* (1986, 1987), and later modifications described by Jackson *et al.* (1990). To improve sensitivity and reduce formation of polyatomic species, the load coil has been modified recently, allowing the sampling distance (load coil to sampler aperture) to be reduced to 13 mm from the factory-supplied configuration of 20 mm. In-house machined aluminum samplers and skimmers and Sciex-type long ICP torches were used for all work reported here.

Operating conditions of the ICP were as for standard solution nebulization (*e.g.*, Jackson *et al.* 1990) except for the inner gas flow (see below). Initial alignment of the instrument was usually performed using solution nebulization. However, optimum inner gas flow and settings of ion lenses for sample introduction *via* the LAM differ significantly from those for solution nebulization owing to the lack of solvent entering the plasma. Optimization of these parameters for LAM use was performed on selected elements in spiked silicate glass NBS (now NIST) standard reference material 612 (referred to as NBS 612) by ablation at 5 Hz using a pulse energy of about 15 mJ. This procedure provides a relatively steady signal (typically about 2000 cps for monoisotopic *REE*) for several minutes without recourse to sample translation. Ion lenses were set to maximize the sensitivity for the heavy elements (> mass 80) with reduced sensitivity for the light elements, including for the most commonly used major-element internal standards.

In the absence of solvent water entering the plasma, levels of polyatomic oxides are reduced but can still be significant for certain analytical applications, notably the determination of concentrations of the *REE*. Generally, maximum sensitivity can be obtained with ThO/Th

less than or equal to 4% (*cf.* typically set to 10% for determination of the *REE* in solutions in our laboratory: Jenner *et al.* 1990). At this level, oxide interferences in the *REE* are negligible for minerals with flat and *HREE*-enriched patterns. For *LREE*-enriched minerals, ThO/Th is further reduced by lowering the inner gas flow to give ThO/Th less than 1% at the cost of reduced sensitivity (typically less than twofold). The selections of the *REE* analytical mass (Table 1) were those suggested by Longerich et al. (1986) for minimum interferences except that the more abundant ^{146}Nd (17%) was preferred to ^{143}Nd (12%) in the absence of a potentially significant interference from ^{130}BaO in the minerals analyzed. No oxide corrections are required under these operating conditions for most minerals.

TABLE 1. DETERMINED IONS AND ISOTOPIC ABUNDANCES

Determined ion	Isotopic abundance (%)	Determined ion	Isotopic abundance (%)
(^{29}Si$^+$)	4.7	^{157}Gd$^+$	15.7
(^{42}Ca$^+$)	0.65	^{159}Tb$^+$	100.0
^{88}Sr$^+$	82.6	^{163}Dy$^+$	24.9
^{89}Y$^+$	51.4	^{165}Ho$^+$	100.0
^{90}Zr$^+$	51.4	^{167}Er$^+$	22.9
^{93}Nb$^+$	100.0	^{169}Tm$^+$	100.0
(^{96}Zr$^+$)	2.8	^{173}Yb$^+$	16.2
^{139}La$^+$	99.9	^{175}Lu$^+$	97.4
^{140}Ce$^+$	88.5	^{178}Hf$^+$	27.2
^{141}Pr$^+$	100.0	^{232}Th$^+$	100.0
^{146}Nd$^+$	17.2	(^{235}U$^+$)	0.72
^{147}Sm$^+$	15.0	^{238}U$^+$	99.3
^{151}Eu$^+$	52.2		

Masses in parentheses used as internal standards.

Data acquisition and reduction

All data were acquired using the multichannel mode of the multi-elements option of the Sciex software. Because of the transient nature of the signals, rapid peak jumping (dwell times of 6–10 ms) was used. Shorter dwell times become unacceptably inefficient owing to quadrupole settling and computer overhead time. Measurement time per point was generally set so that one point was recorded per second for each element (*e.g.*, measurement time per point of 50 ms was used for the determination of 20 elements). The data were buffered during collection to minimize computer overhead.

Background levels for each element were established by acquiring data for approximately 60 s prior to commencing ablation. Ablation of minerals for quantitative analysis was performed at 10 Hz. The laser was generally fired for only 15 s, since the beam typically bores through a standard 30 μm thin section in 15–20 s. For improved precision, longer times can be used on thicker sections at the expense of degraded spatial resolution, both vertical and horizontal (see later for measurements of precision for different volumes of ablation). The total time for data acquisition per analysis was 2 minutes.

The data were transmitted to a remote PC and processed using spreadsheets. The mean intensity of the background was calculated from count-rate data for each element during the preablation period of data acquisition. The sample intensity for each element was then calculated as the mean count-rate during the ablation signal [see Longerich *et al.* (1993) for a typical ablation signal]; we rejected the first point (to minimize contributions from surface contamination) and the tail of the signal (data after intensities fell to less than 50% of the maximum). The net background-corrected intensities were then calculated.

RESULTS AND DISCUSSION

Ablation of minerals

The applications of a microprobe technique are dependent upon its resolution. Other trace microprobe techniques such as SIMS produce pit diameters in the range 2–10 μm (Reed 1990). By contrast, most reports of laser sampling for ICP–MS describe pits in the > 100 μm range (*e.g.*, Gray 1985, Arrowsmith & Hughes 1988, Hager 1989, Remond *et al.* 1990). Furthermore, many rock-forming minerals are particularly difficult to ablate controllably because internal fractures, inclusions, and cleavages act as laser-absorbing features and points of weakness that render them less resistant to the thermomechanical stresses of laser ablation (Fig. 2). From a consideration of the controls of the ablation process, a laser ablation sampling system and operating procedures have been developed that allow the routine production
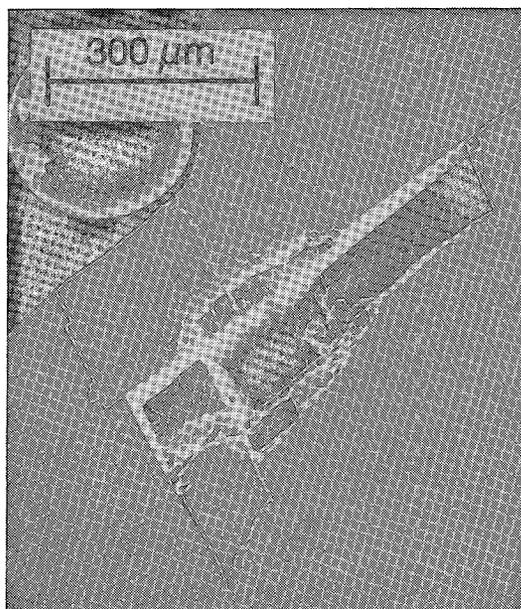
FIG. 2. Scanning electron micrograph of a laser ablation pit in calcite. Note the large rhombic pit around the point of laser focus resulting from cleavage-controlled flaking of the mineral surface.
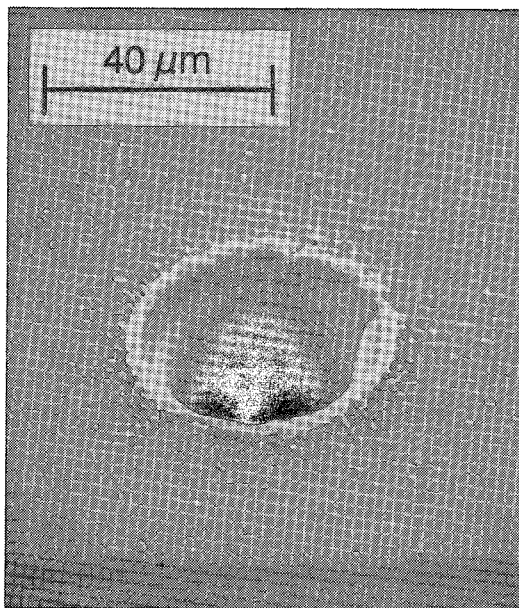
FIG. 3. Scanning electron micrograph of a laser ablation pit 35 μm in diameter in zircon resulting from a 15-s ablation. Solidified droplets of melt ejected during ablation surround the pit.

of pit diameters in the 20–40 μm range for many minerals (Fig. 3). The major controls of the ablation process are mineral structure and chemistry, pulse energy, sample mounting, and the focusing optics.

Mineral structure and chemistry: Minerals display a wide range of responses to ablation, which are related to the degree to which they absorb laser radiation (elemental composition, cleavage, defects, and inclusions) and to their ability to withstand the thermomechanical stress of ablation (brittleness, cleavage, fractures, etc.). Controlled ablation and the formation of small pits seem to occur most readily when absorption occurs near the mineral surface, promoting formation of a plasma that sputters material from the sample surface. Uncontrolled ablation (uncontrolled flaking of large pieces from the mineral surface, with resultant formation of large ragged pits) occurs when sufficient energy is absorbed beneath the mineral surface to cause rupturing and flaking of the crystal.

Minerals have widely differing absorptivity in the near-infrared (Burns 1970), in which the fundamental wavelength of the Nd:YAG laser lies. The absorption of radiation in the visible and near-infrared regions of the electromagnetic spectrum is primarily due to the crystal-field splitting of the energy levels of transition elements, from which minerals obtain their color. Nd:YAG radiation is strongly absorbed by the Fe^{2+} absorption band (Burns 1970), the absorptivity being dependent on the crystallographic orientation of the mineral being ablated. Absorbing minerals require relatively low energies to initiate ablation, and they attenuate the transmitted energy rapidly below the mineral surface, which reduces the likelihood of catastrophic absorption within the crystal. Consequently, these minerals generally ablate controllably. For minerals that absorb less strongly, the ablation response is increasingly controlled by inhomogenities within the mineral; notable are physical features such as defects, cleavages, and inclusions that act as sites of laser absorption beneath the mineral surface that can cause uncontrolled ablation. Fluid inclusions, in particular, can cause severe uncontrolled ablation if ruptured, due to their high overpressures.

Pulse energy: Laser sampling of minerals at pulse energies routinely used in commercial laser ablation systems (10–500 mJ, Denoyer et al. 1991) generally produces instant uncontrolled ablation, which essentially prohibits acquisition of useful data. For controlled ablation and the smallest possible pits, ablation is performed at pulse energies just above the minimum required to promote plasma formation. This varies significantly for different minerals depending upon their absorption characteristics. The optimum condition for each analysis is easily found by initiating laser firing at minimal pulse energy and increasing it with the optical attenuator until ablation commences. Ablation thresholds were found to range from about 0.3–0.5 mJ for the most strongly absorbing minerals (e.g., Fe-rich garnet,

titanite, uraninite) to approximately 2 mJ for weakly absorbing minerals (e.g, quartz, calcite) under the laser operating and focusing conditions used. Use of an internal standard allows variations of the pulse energy during the ablation event without degrading the accuracy of the analytical results.

Sample mounting: Colorless, transition-element-poor minerals with low absorptivity at 1064 nm require relatively high pulse energies to initiate ablation. In standard thin sections, the large transmitted component may be absorbed at the mineral – epoxy – glass slide interface, resulting in the uncontrolled formation of large (up to 0.5 mm), ragged, saucer-shaped pits (Fig. 4). This generally occurs too abruptly to permit useful acquisition of data. However, with the exception of highly cleaved (e.g., fluorite, calcite) or inclusion-rich minerals, satisfactory ablation can generally be achieved in unsupported polished wafers of the type commonly prepared for fluid inclusion studies.

This problem is less severe in absorbing minerals, which require lower pulse energies to promote ablation and more rapidly attenuate the transmitted component. Small cylindrical pits can be produced in thin sections
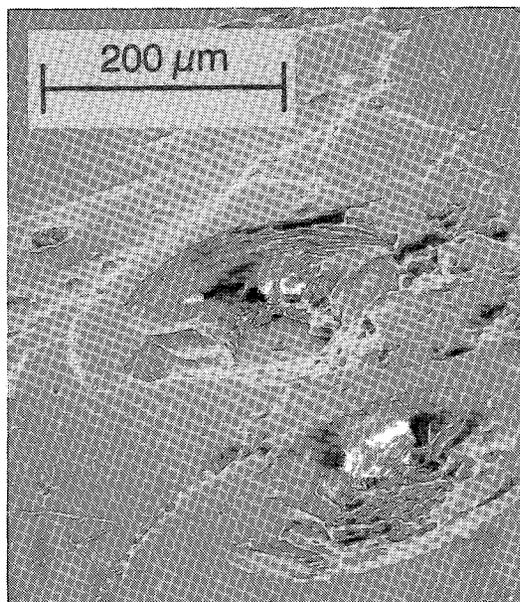
FIG. 4. Scanning electron micrograph of laser ablation pits in a standard thin section of quartz. Melt textures at the base of the pits are the result of absorption at the mineral – glass slide interface (visible in the upper pit). This results in catastrophic ablation and formation of ragged saucer-shaped pits many times the diameter of the laser beam.

of minerals with high absorptivity, particularly if the section is slightly thicker than the standard of 30 μm.

A few minerals ablate uncontrollably regardless of nature of mounting and, in some cases, concentration of transition elements. For example, siderite and rhodochrosite commonly produce large, generally rhombic craters many times the diameter of the incident beam as a result of near-surface rupturing along cleavage planes. This presumably reflects a low resistance to the thermomechanical stress of the ablation event due to the prominent cleavage.

Focusing optics: Characteristics of the ablation pit differ significantly with the type and power of focusing lens. Initial work was performed with singlet lenses. However, for mineral ablation, microscope objective lenses were found to produce superior, cleaner, rounder and smaller pits. Pit diameters and geometries were found to vary with magnification. A 20× objective typically produced cylindrical pits 20–40 μm in diameter, whereas the 5× objective resulted in hemispherical pits 70–80 μm across. Although these complex cemented lenses are much more susceptible to laser-induced damage than singlet lenses, no damage was sustained at pulse energies typically used for ablation of minerals. A simple lens was used for the ablation of NBS glasses, where pit diameter and shape are not important, because their low absorptivity necessitates that much higher pulse energies be used for ablation. The ability to control pit size has important implications for the precision and detection limits (see below).

Quantitative trace-element analysis of minerals

A calibration procedure has been developed for the determination of concentrations of a wide range of trace elements in various minerals. The procedure employs a spiked silicate glass, NBS 612, as a calibration standard

TABLE 2a. CHEMICAL COMPOSITION OF NBS 612 GLASS

SiO_2	71.5	MgO	0.02
TiO_2	0.00	CaO	11.4
Al_2O_3	2.15	Na_2O	13.0
Fe_2O_3	0.03	K_2O	0.02
MnO	0.00	LOI	0.63
		Total	98.80

Atomic absorption analysis; one determination; all results in weight percent.

and uses certain major elements as internal standards to correct for differences in ablation yield, matrix effects, and instrumental drift. NBS 612 is a synthetic silicate glass (Table 2a) that has been spiked with 61 elements at a nominal concentration of 50 ppm. For elements of interest with no certified values, a wafer was analyzed for 32 trace elements (Table 2b) using our standard ICP–MS procedure for silicate samples (Jenner *et al.* 1990). In order to calibrate the LAM, a wafer was mounted in epoxy resin and polished. Calibration involved analyzing NBS 612 for four minutes before and after analyzing a mineral unknown. Because of the extremely low absorptivity of the glass, a pulse energy of about 15 mJ typically was used. To correct for differences in ablation yield, one or more major-element internal standards were determined along with the elements of interest. The elements Si and Ca were found to be the most widely applicable because they occur in many minerals at concentrations sufficient for accurate independent determination by electron microprobe or stoichiometric calculations. They also possess low-abundance isotopes allowing determination by LAM–ICP–MS without saturating the detector. Owing to the mass dependency of matrix effects and signal drift in ICP–MS analysis, Ca was preferred to Si, where possible, because of its closer proximity to the mass of the

TABLE 2b. CHEMICAL COMPOSITION OF NBS 612 GLASS

	N	PPM	SD	RSD		N	PPM	SD	RSD
Li	4	39.9	4.4	11%	Eu	4	34.4	1.0	3%
Be	4	39.0	5.6	14%	Gd	4	35.4	3.0	8%
V	3	37.6	0.3	1%	Tb	4	36.9	0.9	2%
Rb	4	31.1	0.4	1%	Dy	4	35.0	1.0	3%
Sr	4	75.3	1.1	2%	Ho	4	37.3	1.2	3%
Y	4	36.6	0.6	2%	Er	4	37.9	1.2	3%
Zr	4	35.2	1.0	3%	Tm	4	37.3	2.6	7%
Nb	2	38.9	0.7	2%	Yb	4	38.1	2.2	6%
Mo	4	33.8	2.9	8%	Lu	4	37.2	1.8	5%
Cs	4	41.8	1.2	3%	Hf	4	37.6	1.0	3%
Ba	4	38.9	0.7	2%	Ta	2	39.3	0.5	1%
La	4	35.7	1.2	3%	Tl	4	14.8	0.3	2%
Ce	4	37.9	2.0	5%	Pb	4	36.6	3.6	10%
Pr	4	37.4	0.8	2%	Bi	4	33.0	1.4	4%
Nd	4	34.6	2.4	7%	Th	4	36.7	1.6	4%
Sm	4	36.8	1.4	4%	U	4	36.9	1.7	5%

Solution nebulization ICP-MS analyses; 2 analyses of each of 2 dissolutions for most elements; N is number of determinations; SD is standard deviation; and RSD is relative standard deviation.

elements of interest. Unfortunately, the concentration of Fe, a heavier and therefore potentially more suitable major-element internal standard, is not sufficiently high in NBS 612 for accurate determination.

Precision, accuracy, and detection limits

The precision and detection limits of LAM–ICP–MS are complex functions of a number of variables. The fundamental variables are the pit volume (hence the mass of material ablated) and the counting time per element for the ablation mass. The pit size is a function of several variables (ablation time, laser intensity, and mineral), and determines the amount of material presented to the ICP for analysis. A larger pit results in higher count-rates and improved detection-limits and precision. As ablation time is generally restricted by sample thickness (thin section) or by required spatial resolution, the counting time per element is largely a function of the number of elements that are determined. Because the quadrupole mass spectrometer is a sequential analyzer, a larger number of elements in an analysis results in proportionally less counting time per element, poorer counting statistics, and, consequently degraded precision and detection limits (detection limit $\propto \sqrt{1/T}$). Therefore, compromises are always required, and there are no single values for these parameters. Similarly, the accuracy of an analysis is dependent upon the mass of material ablated, and the counting time per element used. The following measurements of precision, accuracy, and detection limits were made for typical analyses where 15–20 elements are determined with good spatial resolution.

Precision

Multiple analyses of a standard thin section of a large (10 × 20 mm diameter) grain of titanite from nepheline syenite pegmatite of the Lillebukt Alkaline Complex (LAC), Stjernøy, Norway (Pedersen *et al.* 1989), demonstrate the precision of the technique. Precision for two pit diameters (30 μm and 75 μm) is shown in Table 3. In each case, a 15-s ablation was used to determine the concentration of 19 trace elements with Ca as the internal standard. During earlier work, the titanite was found to show small concentration-gradients. Therefore, to reduce variation related to chemical inhomogeneity within the grain, the two sets of analyses were performed within very small areas (approximately 1 mm²).

Relative standard deviations (RSD) show an increase (Table 3) at lower concentrations and for isotopes with lower abundance (Table 1) due to poorer Poisson (counting) statistics as concentrations approach the detection limit. The larger spot-size generally has better precision as a result of ablation of more material, and consequently higher count-rates resulting in improved counting statistics. Even at the smaller spot-size, RSDs

TABLE 3. PRECISION OF ELEMENT CONCENTRATIONS IN LAC TITANITE OBTAINED BY LAM-ICP-MS FOR 30 AND 75 μM PIT DIAMETERS

	30 μm pit diameter			75 μm pit diameter		
	MEAN	SD	RSD	MEAN	SD	RSD
Sr	214	10	4%	238	9	4%
Y	443	29	6%	526	24	4%
Zr	2187	197	9%	2301	100	4%
La	383	24	6%	467	31	7%
Ce	1370	69	5%	1570	115	7%
Pr	215	10	4%	251	20	8%
Nd	960	36	4%	1081	71	7%
Sm	228	18	8%	264	10	4%
Eu	70	5	7%	82	6	7%
Gd	176	13	7%	205	11	6%
Tb	25.9	2.4	9%	32.4	2.0	6%
Dy	142	16	11%	163	13	8%
Ho	20.2	2.3	11%	25	3	12%
Er	46	8	18%	54	8	15%
Tm	5.2	1.6	29%	5.9	0.9	15%
Yb	26	5	19%	31	3	10%
Lu	2.7	0.6	22%	3.0	0.6	19%
Th	201	17	8%	208	18	9%
U	18.7	2.7	14%	18.6	1.9	10%

10 analyses for each pit diameter. MEAN = mean concentration in ppm, SD = standard deviation, RSD = relative standard deviation.

are generally less than 10% for concentrations greater than 50 ppm. Considering that, owing to elemental inhomogeneity within the crystal, these RSDs represent maximum values for the analytical technique, they demonstrate a precision useful for geological applications.

Accuracy

The accuracy of the procedure has been established by analyzing separates of a wide variety of minerals (silicates, phosphates, and oxides) for the *REE* and selected other trace elements. For comparison, aliquots of the same separates were analyzed by our standard solution–ICP–MS procedure (Jenner *et al.* 1990). Separates were concentrated by standard techniques of mineral separation and finally hand-picked to achieve near 100% purity. Aliquots for solution analysis ranged from 2 to 16 mg. All the minerals studied are inhomogeneous at the trace-element level.

Titanite: Ten analyses of the LAC titanite (thin section) described above were made at randomly selected points over the section in order to average out chemical inhomogeneities. Pit diameters were approximately 30 μm. The major element Ca was used as the internal standard. Comparisons between solution- and LAM–ICP–MS data are presented in Table 4 and Figure 5. Good agreement exists for most elements. Significant disagreements, where present, are related clearly, to a large extent, to chemical inhomogeneity within the crystal, as indicated by high values of RSD (notably Th and U).

TABLE 4. COMPARISON OF TRACE ELEMENT
CONCENTRATIONS BY LAM- AND SOLUTION-ICP-MS FOR
LAC TITANITE

	SOLN	LAM	SD	RSD	DIFF
Sr	201	209	31	15%	-4%
Y	531	488	50	10%	8%
Zr	2312	2081	601	29%	10%
Th	281	209	90	43%	26%
U	8	19	9	50%	-146%
La	556	445	50	11%	20%
Ce	1846	1546	148	10%	16%
Pr	278	231	32	14%	17%
Nd	1163	1052	146	14%	10%
Sm	256	232	21	9%	10%
Eu	79	78	13	17%	2%
Gd	209	192	27	14%	8%
Tb	30	30	4	15%	-2%
Dy	158	150	23	16%	5%
Ho	25	23	3	12%	8%
Er	55	51	7	14%	7%
Tm	6.5	5.6	1.1	19%	14%
Yb	32	30	6	19%	3%
Lu	3.4	3.3	1.7	53%	4%

All concentrations in ppm; 10 analyses by LAM-ICP-MS. SOLN =
results of a single analysis by solution-ICP-MS; DIFF = relative
difference between solution and LAM-ICP-MS values; other
abbreviations as in Table 3.

Zircon: Several grains of zircon (200–400 µm fraction) from trondhjemite of the Annieopsquotch ophiolite, Newfoundland, were mounted in epoxy resin and polished. Six analyses were made by LAM–ICP–MS, including core and rim areas of the grains using Zr as the internal standard. Pit sizes ranged from 30 to 45 µm. Comparisons between LAM- and solution-ICP–MS and neutron activation analyses of the same separate (Heaman *et al.* 1990) are presented in Figure 6 and Table 5. The high values of the RSDs, which are generally larger than those for the titanite, are due to the large contribution to the variance by sample heterogeneity. Good agreement exists among the three sets of analyses for most elements.

Apatite: Several large grains (100–200 µm) of apatite from the Gaultois granite, Newfoundland, were mounted in epoxy resin and polished. Because of this mineral's extremely low absorption, most grains ablated uncontrollably, and rapid partial or complete destruction of the grains resulted, despite the large grain-size. Four of the six grains analyzed ablated sufficiently well to provide useful data. Comparisons of LAM- and solution-ICP–MS data are presented in Figure 7 and Table 6. The high values of the RSDs indicate that the grains are very heterogeneous. This is reflected by the relatively poor agreement between solution- and average LAM–ICP–MS values compared to the titanite and zircon, although one individual analysis showed near perfect
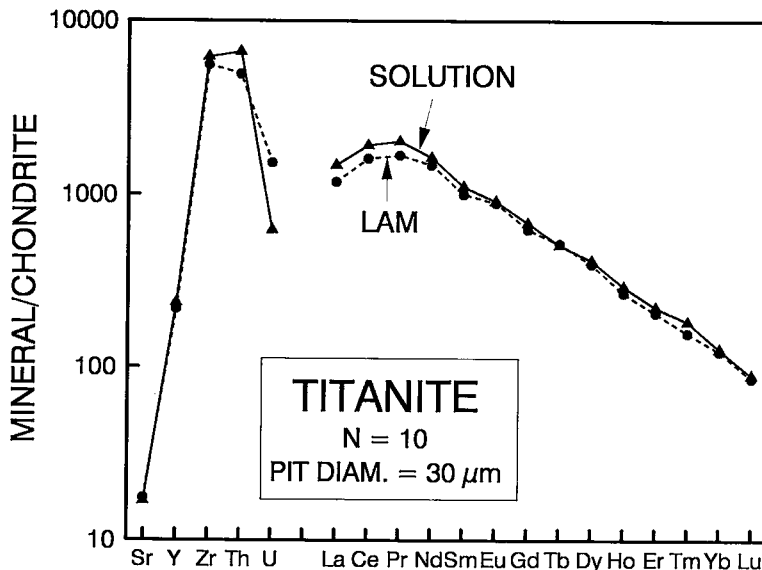
FIG. 5. Comparison of LAM- and solution-ICP–MS data for LAC titanite.
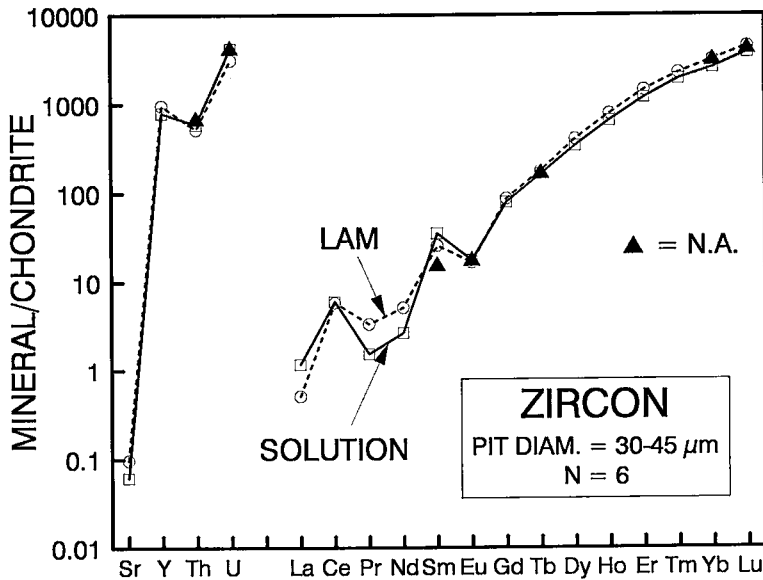
FIG. 6. Comparison of neutron activation (N.A.), and LAM- and solution-ICP–MS data for the zircon separate from the Annieopsquotch trondhjemite.

agreement with the solution-ICP–MS data. Despite the differences in *REE* abundances between analyses, the shapes of the *REE* patterns obtained from the four LAM- and solution-ICP–MS analyses are remarkably similar.

Uraninite: Five analyses were made randomly over a large (1 cm diameter) massive crystal of uraninite in a polished section of ore from the Collins Bay uranium deposit, Saskatchewan. The concentration of U, determined by semiquantitative electron-microprobe analysis, was used for internal standardization. Three separates from the same grain were analyzed by solution-ICP–MS in duplicate. Comparisons of LAM- and solution-ICP–MS data are presented in Figure 8 and

TABLE 5. COMPARISON OF TRACE ELEMENT CONCENTRATIONS BY NEUTRON ACTIVATION, AND LAM- AND SOLUTION-ICP-MS FOR ANNIEOPSQUOTCH ZIRCON

	NA	SOLN	LAM	SD	RSD	DIFF
Sr		0.7	1.2	0.7	63%	58%
Y		1783	2156	554	26%	21%
Hf	10170	9535	8884	480	5%	-7%
Th	28	25	22	10	47%	-12%
U	50	51	38	8	21%	-26%
La		0.4	0.2	0.3	130%	-56%
Ce		5.8	5.6	2.3	42%	-3%
Pr		0.2	0.5	0.3	63%	117%
Nd		1.9	3.7	1.1	29%	93%
Sm	3.5	8.2	6.0	1.5	25%	-27%
Eu	1.5	1.5	1.5	1.0	68%	-5%
Gd		24	27	10	39%	9%
Tb	9.5	10	10	4	41%	9%
Dy		130	155	54	35%	19%
Ho		56	67	20	30%	20%
Er		295	357	100	28%	21%
Tm		68	80	20	26%	17%
Yb	752	633	775	163	21%	22%
Lu	155	143	168	33	20%	17%

All concentrations in ppm; 6 analyses by LAM-ICP-MS. NA = Neutron Activation data; other abbreviations as in Tables 3 and 4.

TABLE 6. COMPARISON OF TRACE ELEMENT CONCENTRATIONS BY LAM-AND SOLUTION-ICP-MS FOR GAULTOIS APATITE.

	SOLN	LAM	SD	RSD	DIFF
Sr	172	152	7	5%	-12%
Y	496	490	84	17%	-1%
Zr	2.0	2.8	1.7	60%	39%
Th	46	28	7	23%	-38%
U	32	22	10	43%	-32%
La	225	183	47	26%	-19%
Ce	734	716	68	9%	-3%
Pr	108	94	13	14%	-13%
Nd	485	380	84	22%	-22%
Sm	101	75	21	28%	-25%
Eu	19	15	4	24%	-21%
Gd	98	80	14	18%	-18%
Tb	12.7	10.4	2.3	22%	-18%
Dy	77	61	7	12%	-20%
Ho	17	12	3	28%	-29%
Er	48	35	9	25%	-28%
Tm	7.1	5.6	1.5	27%	-22%
Yb	45	37	10	26%	-18%
Lu	7.6	6.2	1.1	18%	-19%

All concentrations in ppm; 4 analyses by LAM-ICP-MS. Abbreviations as in Table 3 and 4.
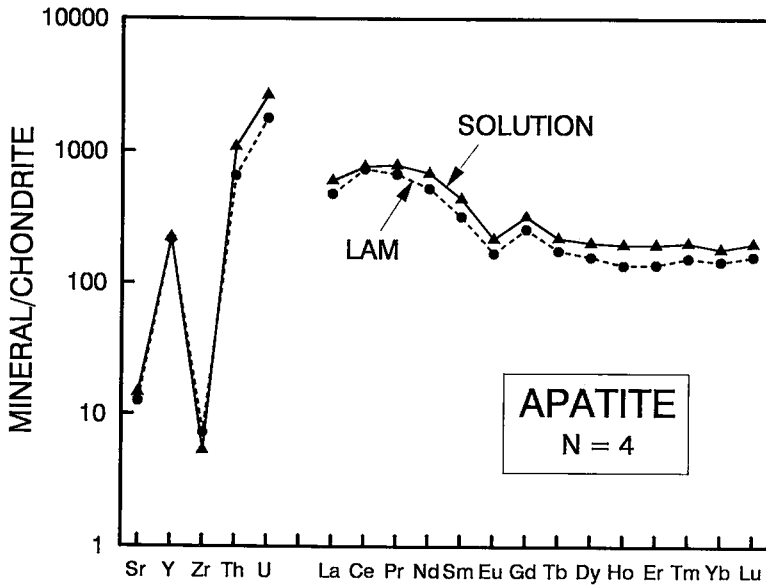
FIG. 7. Comparison of LAM- and solution-ICP–MS data for the apatite separated from the Gaultois granite.

Table 7. Again, the LAM–ICP–MS data indicate the presence of compositional zonation, particularly involving the *LREE*. Despite the very considerable difference in matrix between the NBS 612 silicate standard and the sample, LAM–ICP–MS has reproduced the unusual *REE* pattern of the uraninite with acceptable accuracy for all elements.

Comparison of solution- and LAM–ICP–MS values for all the minerals analyzed is complicated by their chemical inhomogeneities. Work is required on homo-
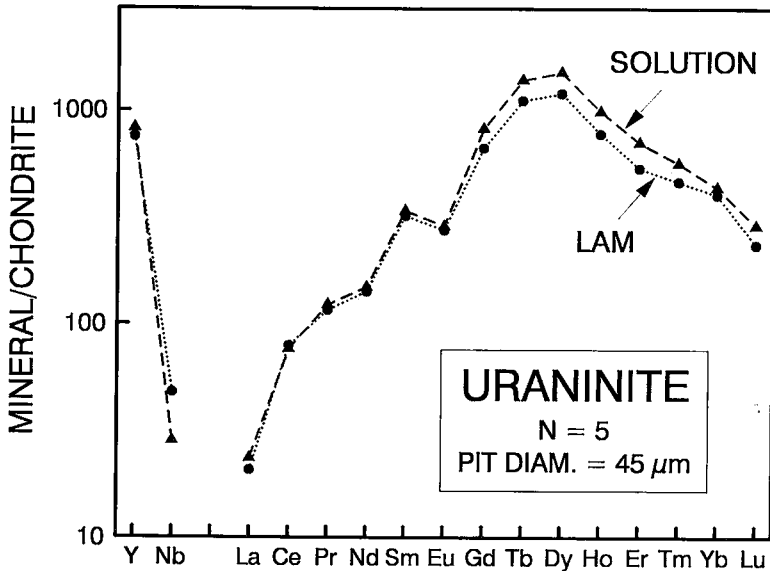
FIG. 8. Comparison of LAM- and solution-ICP–MS data for Collins Bay uraninite.

TABLE 7. COMPARISON OF TRACE ELEMENT CONCENTRATIONS BY LAM- AND
SOLUTION-ICP-MS FOR COLLINS BAY URANINITE

	Solution			LAM			
	MEAN	SD	RSD	MEAN	SD	RSD	DIFF
Y	1855	177	10%	1700	188	11%	-8%
Nb	11	5	48%	18	6	31%	69%
La	8.8	1.2	14%	7.8	2.1	27%	-12%
Ce	73	5	7%	76	205	26%	4%
Pr	16.9	1.1	7%	16	4	27%	-6%
Nd	106	7	7%	101	23	23%	-5%
Sm	78	7	8%	74	11	15%	-5%
Eu	25	1.1	5%	24	5	20%	-4%
Gd	253	18	7%	205	35	17%	-19%
Tb	81	6	8%	65	4	6%	-20%
Dy	574	47	8%	458	19	4%	-20%
Ho	84	7	8%	66	4	6%	-21%
Er	176	15	9%	134	8	6%	-24%
Tm	20.2	1.6	8%	16.6	0.5	3%	-18%
Yb	108	8	7%	100	3	3%	-8%
Lu	11.0	0.8	8%	8.9	0.6	7%	-18%

All results in ppm; solution-ICP-MS data are for duplicate analyses of 3 separates; LAM-ICP-MS
data are for 5 analyses. Abbreviations as in Table 3 and 4.

geneous minerals, either natural or synthetic, to further
verify the calibration strategy. However, the data sug-
gest that the procedure for LAM–ICP–MS calibration
provides results with an accuracy that is quite acceptable
for most geological applications.

Detection limits

Like precision, the detection limits of the LAM–ICP–
MS are a function of the amount of material presented
to the ICP for analysis (pit size) and counting time per

element (number of elements determined for a given
volume of ablation). Thus the detection limits vary,
depending on the parameters selected, and a compromise
for each analysis is required. Estimates of detection
limits for two contrasting sets of analytical parameters
are illustrated; first, the determination of a single,
monoisotopic element in a large volume of ablation, and
secondly, the determination of a large number of
elements at optimum spatial resolution.

A minimum limit of detection obtainable for a single
monoisotopic element in a relatively large volume of
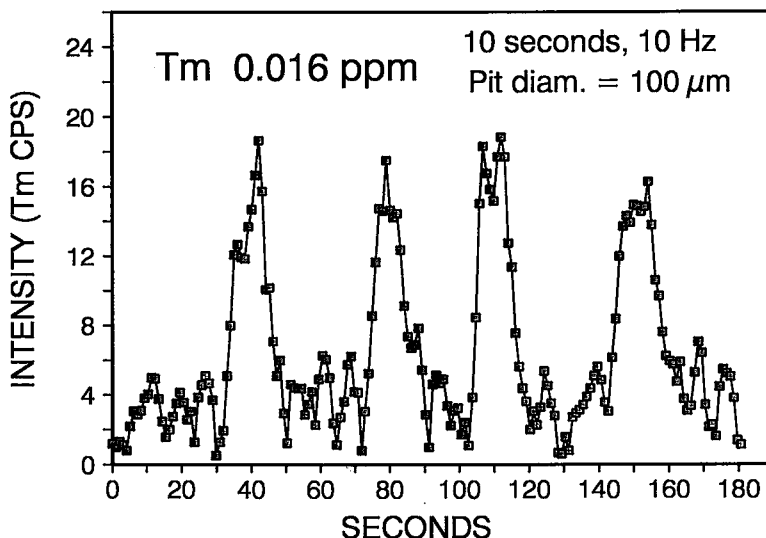
FIG. 9. Signal for Tm (0.016 ppm) for 10-s ablations of NBS 616 silicate glass at intervals
of approximately 40 s. Data smoothed using a 7-point quadratic smoothing function
(Savitzky & Golay 1964). Calculated limit of detection is 0.007 ppm.
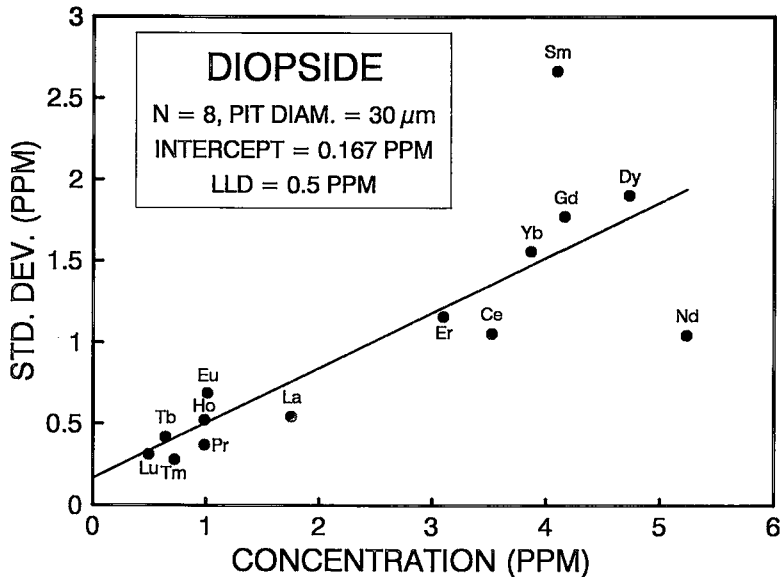
FIG. 10. Standard deviation *versus* concentration plot for eight determinations of the *REE* in diopside by LAM–ICP–MS. Calculated average limit of detection is 0.5 ppm (3 times the standard deviation of a determination at 0 ppm). Deviation of the data points for Nd and Sm from the regression line is due, in part, to the low isotopic abundances of the measured isotopes of these elements.

ablation was demonstrated by the determination of Tm in NBS 616 silica glass (Tm concentration determined as 0.016 ppm by solution-ICP–MS). Ablation was performed at 15 mJ/pulse for 10-s periods at approximately 40-s intervals. The resulting ablation pits were approximately 100 µm in diameter. Clear and reproducible signals were obtained (Fig. 9). The calculated limit of detection (3 standard deviations of the background) was 0.007 ppm.

An estimate of the detection limit that applies in determinations of numerous elements at high spatial resolution was obtained from the precisions of eight determinations of the complete set of *REE* in a homogeneous crystal of diopside. For each analysis, ablation was performed for 15 s at approximately 1 mJ/pulse. Resultant pit diameters were approximately 30 µm, close to the smallest spatial resolution obtained in this study. Using linear regression (Fig. 10), an average detection limit of 0.5 ppm was estimated (noting that no account was taken of the different isotopic abundances of the measured isotopes).

Application to the study of chemical zoning in minerals

Most of the minerals studied exhibit pronounced zonation in the distribution of the trace elements. In order to demonstrate the potential of LAM–ICP–MS to the study of trace-element zoning in minerals,
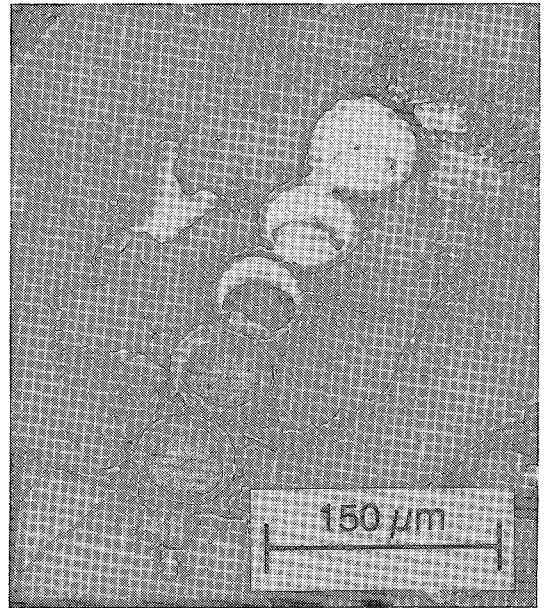
FIG. 11. Scanning electron micrograph of a 5-point laser-ablation sampling traverse across a grain of garnet from the Preissac–Lacorne batholith. Each 45-µm-diameter pit is the product of a 20-s ablation.
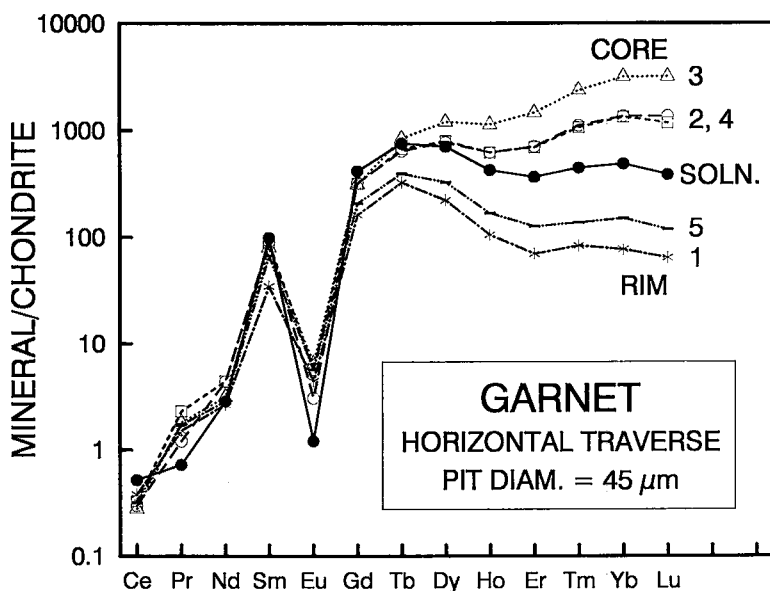
FIG. 12. Chondrite-normalized *REE* patterns (five determinations) from the lateral sampling traverse of a grain of garnet from the Preissac–Lacorne batholith. Solution analysis (SOLN.) also is shown.

an extensive study has been made of a garnet separate which appeared, from preliminary trace-element analytical data, to be very strongly zoned. In addition to performing lateral sampling, the ability of the LAM to bore, and produce vertical elemental profiles at finer spatial resolution, was examined.

The garnet is a Mn-rich hydrothermal phase from the alteration envelopes surrounding quartz veins related to molybdenum mineralization in the Preissac–Lacorne batholith, Quebec. Electron-microprobe analyses indicated no significant zonation of the major elements (typical compositions, core: $Sps_{57.1}Alm_{40.2}Grs_{2.3}Prp_{0.5}$, rim: $Sps_{56.4}Alm_{40.8}Grs_{2.1}Prp_{0.7}$). Several grains of garnet from the 200–600 μm fraction were mounted in epoxy resin and polished down to their core. A 5-point traverse was made across one grain 250 μm in diameter. Figure 11 shows the ability of the LAM to make round, cylindrical pits at close proximity, as required for a lateral traverse. Ablation times were 20 s, and pit

TABLE 8. CONCENTRATION PROFILES FOR REE BY LAM-ICP-MS FOR GARNET GRAINS FROM THE PREISSAC-LACORNE BATHOLITH

	Solution	Horizontal Traverse					Vertical Traverse				
		1	2	3	4	5	1	2	3	4	5
La	0.1	0.5	0.2	0.4	0.3	0.1	0.1	0.1	0.2	0.4	0.3
Ce	0.5	0.4	0.3	0.3	0.3	0.3	0.2	0.3	0.2	0.5	0.3
Pr	0.1	0.2	0.3	0.2	0.2	0.2	0.2	0.2	0.2	0.3	0.5
Nd	2.0	1.9	3.1	2.2	3.1	2.0	2.4	2.1	2.3	3.1	4.4
Sm	22.7	8.0	20.6	18.5	21.1	15.5	18.5	16.6	15.7	18.0	21.0
Eu	0.1	0.4	0.5	0.6	0.3	0.5	0.2	0.3	0.4	0.3	0.9
Gd	126	49	97	95	98	63	102	83	65	64	57
Tb	44	19	39	49	37	23	47	34	25	23	18
Dy	268	84	302	457	293	124	398	276	177	137	109
Ho	36.1	8.9	52.7	96.5	52.7	14.3	76.7	50.1	25.9	18.1	12.2
Er	91	17	172	364	175	31	258	159	69	44	32
Tm	15.9	2.9	37.8	84.3	39.4	4.9	55.0	32.1	12.5	7.7	5.0
Yb	120	19	330	785	335	37	467	287	102	57	34
Lu	14.6	2.4	44.6	121.1	51.6	4.5	66.0	37.8	12.8	6.1	4.0

All concentrations in ppm; solution-ICP-MS data are the mean values for single analyses of 2 separates.
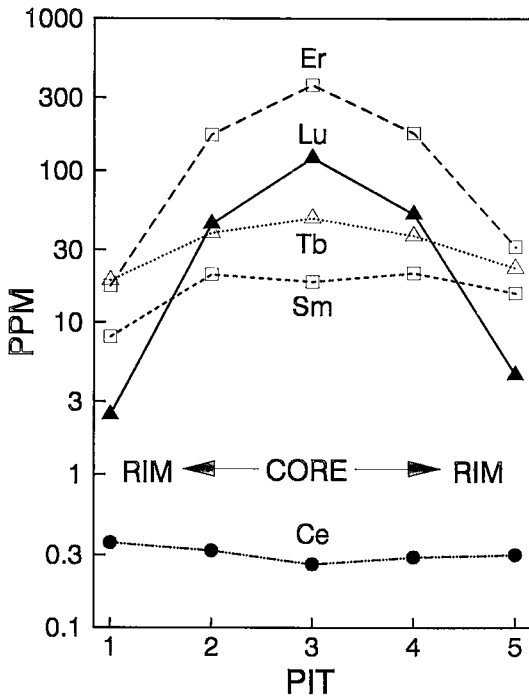
FIG. 13. Profiles of elemental concentrations for selected *REE* for the 5-point lateral analytical traverse of a grain of garnet from the Preissac–Lacorne batholith.
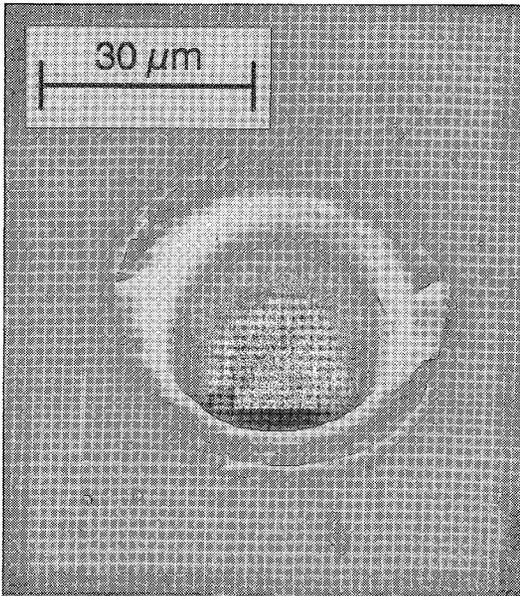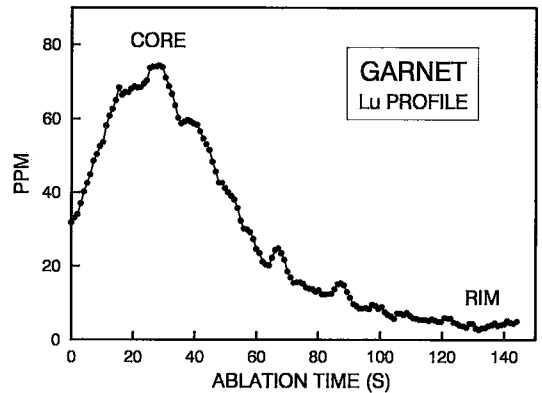
FIG. 15. Vertical chemical profile for Lu in a grain of garnet from the Preissac–Lacorne batholith. Data smoothed using a 9-point quadratic smoothing filter (Savitzky & Golay 1964). Each point represents approximately 1 μm.

diameters approximately 45 μm. Silicon was used for internal standardization.

Chondrite-normalized *REE* patterns for the five spots and the solution–ICP–MS analysis of the mineral digest are presented in Figure 12 and Table 8. Lateral profiles of concentration for five selected elements are shown in Figure 13. The technique demonstrates almost two orders of magnitude variation in abundances of the heavy *REE* between the core and rim of a grain that showed no significant variation in major-element abundances. Note that the solution analysis gives the mean concentration for the separate.

The cylindrical pits attainable with the LAM (Fig. 14) suggest that it could be used to bore through grains and thereby produce vertical chemical profiles. To demonstrate this ability, *REE* data were collected from a garnet grain 250 μm in diameter during a 3-minute period of ablation, during which the laser bored from the core to the rim of the grain. The resulting pit diameter was approximately 75 μm.

A profile of concentration *versus* time for Lu is presented in Figure 15. It is not known exactly at what time the laser beam penetrated the lower edge of the grain or whether the rate of boring remained constant throughout the ablation period. However, it is evident that the average rate of boring was approximately 1 μm/s. Data points therefore represent about 1 μm vertical resolution. Again, extreme enrichment in the *HREE* in the core of the grain of garnet relative to its rim is evident. The initial rise in Lu concentrations with depth indicates that the polished surface was above the grain's core. The smaller range of Lu concentrations compared to that found in the lateral traverse is due, in part, to a dilution effect caused by ablation of material from the pit walls, as indicated by the large diameter of the pit compared to the pits of the lateral traverse.

FIG. 14. Scanning electron micrograph of a laser ablation pit in diopside showing the ability of the LAM to bore cylindrical pits suitable for vertical profiling.
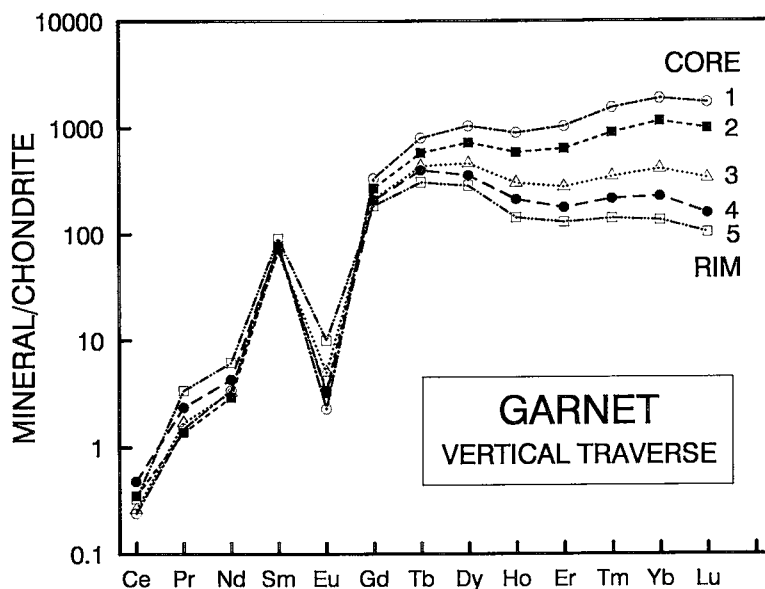
FIG. 16. Chondrite-normalized *REE* patterns representing 30-s (approximately 30 µm) intervals of a vertical ablation traverse through a grain of garnet from the Preissac–Lacorne batholith.

By integrating the data for all of the *REE* over selected intervals, chondrite-normalized patterns can be prepared for any sampling interval. *REE* patterns obtained by integrating the data from 75 to 225 s in 30-s increments are presented in Figure 16 and Table 8. Each composition pertains to approximately a 30-µm depth interval.

CONCLUSIONS

For many analytical applications, ICP–MS has superseded previous analytical techniques in terms of speed, sensitivity, and elemental coverage. The coupling of a LAM to an ICP–MS is straightforward and inexpensive. The resulting microprobe technique is capable of rapid, precise, and accurate determination of concentrations of trace elements in many minerals. Interferences are not problematic, and calibration is very straightforward. With current resolution in the 20–40 µm range for many minerals, and detection limits less than 1 ppm for many elements, the technique rivals competing microprobe techniques in its analytical capabilities. Design improvements in the sample cell and transfer system and the improved sensitivity of the latest generation of ICP–MS instruments should allow substantial reductions in detection limits. Use of different wavelengths of the laser also can be expected to allow further improvement in spatial resolution, particularly for minerals with low absorptivity at 1064 nm. In addition, the ability of the LAM to bore provides the technique with the potential to produce vertical chemical profiles with spatial resolution of a few micrometers.

For the igneous petrologist, this resolution will permit tests of mineral:melt partition coefficients and their variation with evolution of the melt, for well-constrained samples. Tests for decoupling of major from trace elements during igneous processes will be possible at the scale of the individual mineral grain. In addition, measurement of the concentrations of the rare earths and other trace elements between coexisting zones (core *versus* rim) in mineral pairs in apparent equilibrium is possible. This will augment the power of the electron microprobe to do the same for the major elements. The combined major- and trace-element data-sets for individual zones of single mineral grains will provide fundamental new information (and likely greater complexity) with which to further assess petrological processes. Important applications for LAM–ICP–MS also are foreseen in the fields of metamorphic, sedimentary and economic geology.

In addition to trace-element analysis of minerals, the technique has the potential to perform *in situ* determinations of isotope ratios (Fryer *et al.* 1991) and analysis of individual fluid inclusions. As a low-cost accessory to the analytically powerful and increasingly widespread ICP–MS, the LAM has the potential to become a widely available tool and thus an important addition to the field of microanalytical geochemistry.

REFERENCES

ARROWSMITH, P. (1987): Laser ablation of solids for elemental analysis by inductively coupled plasma mass spectrometry. *Anal. Chem.* **59**, 1437-1444.

_____ & HUGUES, S.K. (1988): Entrainment and transport of laser ablated plumes for subsequent elemental analysis. *Appl. Spectros.* **42**, 1231-1239.

BEAUCHEMIN, D. & CRAIG, J.M. (1990): Investigation on mixed gas plasmas produced using a sheathing device in ICP–MS. *In* Plasma Source Mass Spectrometry. Proc. Third Surrey Conf. on Plasma Source Mass Spectrometry (K.E. Jarvis, A.L. Gray, I. Jarvis & J. Williams, eds.). The Royal Society of Chemistry, Cambridge, England (25-42).

BURNS, R.G. (1970): *Mineralogical Applications of Crystal Field Theory.* Cambridge University Press, London.

DENOYER, E.R., FREDEEN, K.J. & HAGER, J.W. (1991): Laser solid sampling for inductively coupled plasma mass spectrometry. *Anal. Chem.* **63**, 445A-457A.

FRYER, B.J., JACKSON, S.E. & LONGERICH, H.P. (1991): In-situ, single grain, U–Pb geochronology by laser ablation ICP–MS: the MUN-Probe. *Terra Abstr.* **3**, 504.

GRAY, A.L. (1985): Solid sample introduction by laser ablation for inductively coupled plasma source mass spectrometry. *Analyst* **110**, 551-556.

HAGER, J.W. (1989): Relative elemental responses for laser ablation-inductively coupled plasma mass spectrometry. *Anal. Chem.* **61**, 1243-1248.

HEAMAN, L.M., BOWINS, R. & CROCKET, J. (1990): The chemical composition of igneous zircon suites: implications for geochemical tracer studies. *Geochim. Cosmochim. Acta* **54**, 1597-1607.

JACKSON, S.E., FRYER, B.J., GOSSE, W., HEALEY, D.C., LONGERICH, H.P. & STRONG, D.F. (1990): Determination of the precious metals in geological materials by inductively coupled plasma-mass spectrometry (ICP–MS) with nickel sulphide fire-assay collection and tellurium coprecipitation. *Chem. Geol.* **83**, 119-132.

JENNER, G.A., LONGERICH, H.P., JACKSON, S.E. & FRYER, B.J. (1990): ICP–MS – a powerful tool for high-precision trace-element analysis in earth sciences: evidence from analysis of selected U.S.G.S. reference samples. *Chem. Geol.* **83**, 133-148.

LONGERICH, H.P., FRYER, B.J., STRONG, D.F. & KANTIPULY, C.J. (1987): Effects of operating conditions on the determination of the rare earth elements by inductively coupled plasma-mass spectrometry (ICP–MS). *Spectrochim. Acta* **42B**, 75-92.

_____, JACKSON, S.E., FRYER, B.J. & STRONG, D.F. (1993): Machinations: the laser ablation microprobe-inductively coupled plasma-mass spectrometer (LAM–ICP–MS). *Geosci. Canada* **20** (in press).

_____, STRONG, D.F. & KANTIPULY, C.J. (1986): Progress in evaluation of instrumental and other parameters affecting chemical and isotopic analysis by inductively coupled plasma-mass spectrometry (ICP–MS). *Can. J. Spectros.* **31**, 111-121.

MOENKE-BLANKENBURG, L., GÄCKLE, M., GÜNTHER, D. & KAMMEL, J. (1990): Processes of laser ablation and vapour transport to the ICP. *In* Plasma Source Mass Spectrometry. Proc. Third Surrey Conf. on Plasma Source Mass Spectrometry (K.E. Jarvis, A.L. Gray, I. Jarvis & J. Williams, eds.). The Royal Society of Chemistry, Cambridge, England (1-17).

PEDERSEN, R.B., DUNNING, G.R. & ROBINS, B. (1989): U–Pb ages of nepheline syenite pegmatites from the Seiland Magmatic Province, N. Norway. *In* The Caledonide Geology of Scandinavia (R.A. Gayer, ed.). Graham and Trotman, London (3-8).

POTTS, P.J. (1987): *A Handbook of Silicate Rock Analysis.* Blackie & Sons, Glasgow.

REED, S.J.B. (1990): Recent developments in geochemical microanalysis. *Chem. Geol.* **83**, 1-9.

REMOND, G., BATEL, A., ROQUES-CARMES, C., WEHBI, D., ABELL, I. & SEROUSSI, G. (1990): Scanning mechanical microscopy of laser ablated volumes related to inductively coupled plasma-mass spectrometry. *Scanning Microscopy* **4**, 249-274.

SAVITZKY, A. & GOLAY, M.J.E. (1964): Smoothing and differentiation of data by simplified least squares procedures. *Anal. Chem.* **36**, 1627-1639.